

Molecular Mechanism of the Cell Membrane Pore Formation Induced by Bubble Stable Cavitation

Viet Hoang Man,[†] Phan Minh Truong,[‡] Mai Suan Li,[§] Junmei Wang,[†] Nguyen-Thi Van-Oanh,^{||} Philippe Derreumaux,^{*,†,‡,§} and Phuong H. Nguyen^{*,†}

[†]Department of Pharmaceutical Sciences, School of Pharmacy, University of Pittsburgh, Pittsburgh, Pennsylvania 15213, United States

[‡]Institute for Computational Science and Technology, SBI Building, Quang Trung Software City, Tan Chanh Hiep Ward, District 12, Ho Chi Minh City, Vietnam

[§]Institute of Physics, Polish Academy of Sciences, Al. Lotnikow 32/46, 02-668 Warsaw, Poland

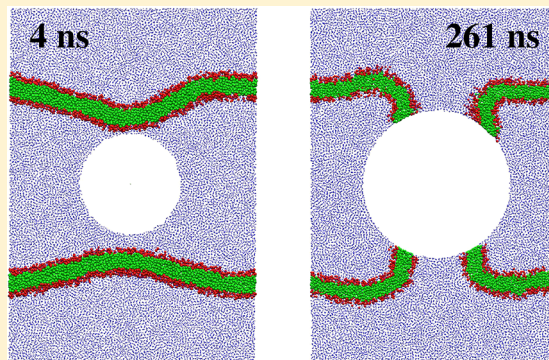
^{||}Laboratoire de Chimie Physique, CNRS, Université Paris Sud, Université Paris-Saclay, 91405 Orsay Cedex, France

[†]Laboratory of Theoretical Chemistry, Ton Duc Thang University, Ho Chi Minh City, Vietnam

^{*}Faculty of Pharmacy, Ton Duc Thang University, Ho Chi Minh City, Vietnam

[†]Laboratoire de Biochimie Théorique, UPR 9080, CNRS, Université Denis Diderot, Sorbonne Paris Cité, IBPC, 13 rue Pierre et Marie Curie, 75005 Paris, France

ABSTRACT: Microbubbles in combination with ultrasound provide a new and promising way to deliver drugs into living cells. It is believed that the stable vibration or the collapse of the bubbles under ultrasound are the two main mechanisms that induce the formation of pores in the cell membranes, through which drugs may get inside the cell cytoplasm. The bubble collapse hypothesis is not only intuitive since released shock waves can easily penetrate and create pores in the membrane, but it is also confirmed by both experiment and theory. In contrast, the molecular mechanism of stable vibration is not well-understood because of experimental difficulties resulting from the fragility of bubbles and the lack of molecular dynamics simulation studies. To obtain a better understanding of this mechanism, we developed a lipid-coated bubble model that we applied to simulate the stable cavitation of the bubble in the presence of a lipid bilayer. We show that the wall shear stress generated by the bubble vibration does not induce the membrane pore formation. Instead, the bubble fuses with the membrane and subsequent cavitation pulls lipid molecules out of the membrane, creating pores. This could help one to choose the best combination of the bubble shell materials, the ultrasound frequency, and intensity, so that the opening and closing of pores will be optimized.



INTRODUCTION

Microbubbles in combination with ultrasound have been used in many fields, such as medicine, pharmacology, material science, and the food industry.¹ A beautiful example is the application in the delivery of drugs into cells.^{2–6} Under ultrasound, bubbles oscillate in size. If the oscillation is slow, then the contraction and expansion of the bubble size are approximately symmetric. This phenomenon is called stable cavitation. It produces a rapid flow of liquid around the bubble and induces shear stress on nearby objects. In contrast, a fast oscillation with large amplitude may lead to asymmetric contraction and expansion followed by a violent collapse called inertial cavitation. This collapse produces shock waves that propagate at supersonic speed radially from the collapse site.⁷ The molecular mechanism of how the bubble cavitation induces the formation of pores in the cell membrane, through which drugs may get inside the cell cytoplasm, is poorly

understood.^{8–11} Some believe that the mechanism requires inertial cavitation,^{12–16} while others contend that stable cavitation is sufficient. In the later case, shear stress associated with acoustic microstreaming is believed to play a key role.^{17–21} Others contend that both types of cavitation are important.²²

From the theoretical side, a number of simulations employing continuum,²³ coarse-grained, and atomistic molecular models^{24–32} have been carried out to study inertial cavitation and the effect the shock waves have on the lipid bilayer structure. These studies have confirmed that inertial cavitation can induce the formation of membrane pores. We have not seen in the literature molecular dynamics (MD)

Received: September 26, 2018

Revised: December 12, 2018

Published: December 12, 2018

simulations aimed at studying the effects of stable cavitation on the membrane. Recently, we have developed a bubble model for MD simulations of stable cavitation.³³ The model has been applied to studying the effects of stable cavitation on amyloid fibrils³³ and to verify the Rayleigh–Plesset equation for the description of the dynamics of nanosized bubbles.³⁴ In those works, the bubble was modeled by an empty water cavity, where a strong time-dependent repulsive potential was applied to maintain and regulate the size of the bubble.

Experimentally, the bubble shell is made from proteins, carbohydrates, phospholipids, or biodegradable polymers. Among these materials, the lipid-coated bubbles do not exhibit sonic cracking and can readily expand and contract during the ultrasound pulse, making them ideal for drug delivery applications.³⁵ Being lipids, these bubbles can also fuse with the lipid bilayer of the cell membrane. Given this, we propose a different mechanism for the drug delivery into cells by bubble cavitation. This mechanism consists of stable cavitation of lipid-coated bubbles that are fused with the cell membrane to induce the formation of pores in the cell membrane. To this end, the core aim of this work is 2-fold, (i) to further develop the previous bubble model to mimic lipid-coated nanobubbles, and (ii) to carry out nonequilibrium MD (NEMD) simulation with this model to verify the proposed mechanism. We will show that the wall shear stress induced by bubble cavitation does not play a key role in the pore formation.

METHODOLOGY

Bubble Model. Our bubble is modeled by a particle which interacts with surrounding atoms by a time-dependent Lennard-Jones potential of the form

$$V[r, \sigma(t)] = \begin{cases} 4\epsilon \left[\left(\frac{\sigma(t)}{r} \right)^{12} - \left(\frac{\sigma(t)}{r} \right)^6 \right], & r \leq \sigma(t) \\ 4\epsilon^* \left[\left(\frac{\sigma(t)}{r} \right)^{12} - \left(\frac{\sigma(t)}{r} \right)^6 \right], & r > \sigma(t) \end{cases} \quad (1)$$

$$(2)$$

where r is the distance between the center of the bubble and a surrounding atom, and $R(t) \equiv \sigma(t)$ is the bubble radius. The repulsive potential with the strength ϵ (eq 1) was used in our previous work^{33,34} to create an empty cavity in a liquid, mimicking a bubble. Equation 2 is new, describing the attractive interaction between the bubble surface with surrounding atoms, and is represented by a mean field attractive strength ϵ^* . To mimic the ultrasound-induced stable cavitation, the time-dependent bubble radius is expressed as a harmonic function

$$R(t) = \frac{(R_{\max} + R_{\min})}{2} + \frac{(R_{\max} - R_{\min})}{2} \sin\left(\frac{2\pi t}{\tau} - \pi\right) \quad (3)$$

where τ is the vibrational period, and R_{\max} and R_{\min} are the maximum and minimum radii, respectively. At $t = 0$, the bubble is at equilibrium with the radius $R_0 = (R_{\max} + R_{\min})/2$. During the simulation, the behavior of a bubble subjected to ultrasound is mimicked by the variation in $R(t)$, which induces a harmonic oscillation in the potential, resulting in the vibration of the size of the bubble. The bubble vibration pushes and pulls surrounding atoms back and forth, thus generating liquid flow around the bubble.

System and Parameters. We studied the membrane composed of 1,2-dioleoyl-*sn*-glycero-3-phosphocholine (DOPC) lipids immersed in water. The coarse-grained MARTINI 2.0 force field^{36,37} was employed to describe the

membrane and water. In this force field, a coarse-grained water bead represents four water molecules. A DOPC lipid molecule consists of hydrophilic (NC3 and PO4) beads, hydrophobic (C1A, D2A, C3A, C4A, C1B, D2B, C3B, and C4B) beads, and intermediate (GL1 and GL2) beads (Figure 1A). MD

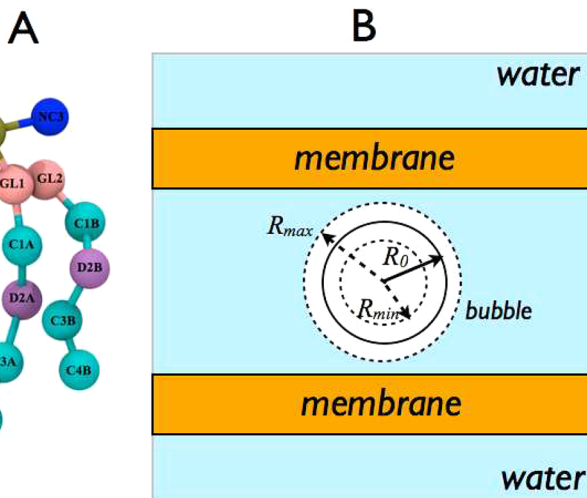


Figure 1. Schematic view of the computational model. (A) The MARTINI coarse-grained DOPC lipid model. (B) The system consists of two DOPC membranes solvated in water. The bubble is modeled as an empty spherical cavity with the equilibrium radius $R_0 = 8$ nm, placed at the center of the simulation box. The bubble radius is allowed to oscillate between $R_{\min} = 4$ nm and $R_{\max} = 12$ nm.

simulations using the MARTINI force field have shown that the fusion of membranes is dominated by the attractive interaction between charged lipid head groups,³⁸ which are the NC3 and PO4 beads shown in Figure 1A. Thus, to account for the interaction between our lipid-coated bubble model with the membrane and water, the mean field interaction strength ϵ^* in eq 2 is estimated as the arithmetic average of the attractive strengths between NC3–NC3 (3.5 kJ/mol), PO4–PO4 (4.99 kJ/mol), NC3–PO4 (4.49 kJ/mol), and between these beads with a water bead (5.59 kJ/mol). This yields $\epsilon^* = 4.64$ kJ/mol. The repulsive strength in eq 1 prevents the collapse of the bubble, thus it can simply take a large value, which was chosen to be $\epsilon = 50$ kJ/mol in this work.

Our system is shown in Figure 1B. It consists of two membranes separated at least 24 nm, and both are solvated in water. Bubble cavitation exerts pressure on the nearby membrane, but the same pressure also acts on another side of the membrane due to the periodic boundary conditions in the MD simulations. The use of two membranes prevents this artifact,³¹ and also doubles the statistics because the two membranes are symmetric. The initial dimensions of the unit cell were (L_x, L_y, L_z) nm. Starting from this configuration, an equilibrium MD simulation was carried out for 50 ns in the NPT ensemble with the pressure $P = 1$ bar and temperature $T = 300$ K, employing the GROMACS simulation package.³⁹ From the last configuration of the NPT equilibration run, a bubble (with a radius R_0 of 8 nm) was formed at the center of the box by removing water molecules within this sphere. The resulting system that was used in our simulations consists of 9184 DOPC lipids and 646991 waters.

Frequency of the Bubble Vibration. The typical radius of a clinically approved bubble for experiments is $R_0 = 0.5\text{--}5$ μm . The frequency of the ultrasound is usually tuned to be $\omega =$

0.5–10 MHz ($\tau = 2\text{--}0.1 \mu\text{s}$), so that resonance with the bubble oscillations occurs, and hence, that the bubble absorbs most of the energy from the ultrasound field. To be computationally feasible with available computer resources, our system size and simulation times were chosen to be on the order of nanometers and nanosecond scales, respectively. This forces the simulated bubble to be nanometric in radius, and for it to vibrate with nanosecond periods. To determine the vibrational frequency for our bubble model, we allowed it to vibrate with a frequency that is equal to the resonance frequency of a gas bubble having the same radius. Since the bubble oscillates freely in the ultrasound field, the resonance frequency is given by⁴⁰

$$\omega = \frac{1}{2\pi} \sqrt{\frac{1}{\rho R_0^2} \left(3\kappa P_0 + 3(\kappa - 1) \frac{2\sigma}{R_0} \right)} \quad (4)$$

Using a water density of $\rho = 10^3 \text{ kg m}^{-3}$, an ambient water pressure of $P_0 = 1 \text{ bar}$, a water–air surface tension of $\sigma = 0.072 \text{ kg s}^{-2}$ at 300 K and 1 bar,⁴¹ and a polytropic index of $\kappa \approx 1$, we obtain from eq 4 a resonance frequency of $\omega = 230 \text{ MHz}$ ($\tau = 4.3 \text{ ns}$) for a bubble with a radius of $R_0 = 8 \text{ nm}$. We used this frequency in all the simulations described in the following sections.

NEMD Simulations of Induced Bubble Cavitation. The GROMACS simulation package³⁹ coupled to our bubble cavitation code was used for all the simulations. An important question remains regarding the appropriate ensemble for the NEMD simulations. That is, should the NEMD simulations be run at constant pressure, at constant temperature, or at constant energy? To help answer this question, one must recall that, in MD simulations, the coupling to the pressure bath or the temperature bath is achieved by rescaling the coordinates or the velocities of all atoms at every time step, such that the desired pressure or temperature is maintained.⁴² In an ultrasound-induced nonequilibrium experiment, on the other hand, the bubble expansion and contraction generate a time-dependent pressure in the system. Coupling the system to the barostat may artificially suppress the variation in the pressure. Thus, one may reason that the NEMD simulations should not be done at constant pressure. Furthermore, bubble cavitation induces water flow in the system, and the rescaling of the velocities of atoms in the simulation may artificially suppress this flow. For this reason, the NEMD simulations should not be done at constant temperature. If the simulations are done at constant energy, then heating occurs in the system due to work done by the bubble cavitation on the water. In the constant energy simulations, the damage of the membrane may be simply due to heat. Taking into account these arguments, we suggest that the appropriate conditions for the NEMD simulations are constant volume with only the membrane coupled to the heat bath. This ensures that the damage to the membrane is not due to heat and that water flow is not suppressed, since water is not directly coupled to the heat bath. In the current study, the membrane is coupled to the heat bath at temperature of 300 K using the Berendsen coupling method⁴² with a temperature coupling constant of 0.1 ps. The equations of motion are integrated using the leapfrog algorithm with a small time step of 10 fs. The electrostatic interactions are calculated using the particle mesh Ewald method and a cutoff of 1.4 nm.⁴³ A cutoff of 1.4 nm is used for the van der Waals interactions. The nonbonded pair lists are updated every 5 fs. The use of a small time step, a more

frequent update of the pair lists, and a large neighboring list ensures that temperature of the water is well-maintained.⁴⁴ During the simulations, the center of the bubble is fixed to the center of the simulation box.

RESULTS AND DISCUSSION

Effect of the Wall Shear Stress on the Formation of a Membrane Pore.

To investigate the role of the bubble oscillation-induced wall shear stress on the membrane, we carried out a 800 ns NEMD simulation in which eq 2 includes only the attractive interaction between the bubble with water but not with the membrane. The bubble radius was allowed to vibrate between $R_{\min} = 4 \text{ nm}$ and $R_{\max} = 12 \text{ nm}$ with a period of $\tau = 4.3 \text{ ns}$. Figure 2A shows the time evolution of the bubble

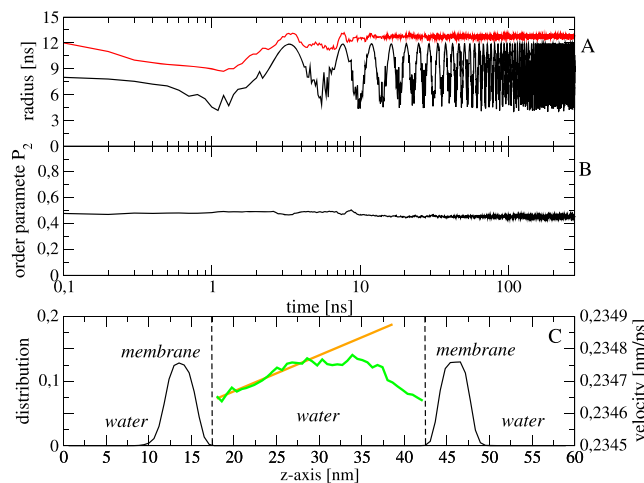


Figure 2. Time evolution of (A) the bubble radius (black) and the shortest distance between the bubble's center to the membrane (red). (B) The lipid order parameter. The distribution along the z -axis of the position of lipid bead (black, left axis) and the average water velocity parallel to the membrane (green, right axis) are shown in (C). The linear data fit of the velocity is shown in orange. For clarity, the x -axis in (A) and (B) is shown by log-scale, and only data points up to 280 ns are shown.

radius $R(t)$ and the shortest distance $D(t)$ between the bubble center and the membrane. The bubble was initially at equilibrium with $R_0 = 8 \text{ nm}$ and $D(t) = 12 \text{ nm}$. Then, it was compressed to its minimum size of $R_{\min} = 4 \text{ nm}$ at $t = \tau/4 = 1.07 \text{ ns}$, which resulted in a slight decrease in $D(t)$, indicating the bending of the membrane. After that, the bubble expands to the equilibrium, $R_0 = 8 \text{ nm}$, and maximum, $R_{\max} = 12 \text{ nm}$, sizes at $t = \tau/2 = 2.15 \text{ ns}$ and $t = 3\tau/4 = 3.22 \text{ ns}$, respectively. During this time, the membrane bends when D increases and reaches a peak value of $\sim 13 \text{ nm}$ at 3.22 ns. Then, the bubble was compressed to its equilibrium size, and the membrane restored to its equilibrium position at $t = \tau = 4.3 \text{ ns}$, finishing one cavitation period. During the next 186 cavitation periods (800 ns trajectory), the membrane was always close to the bubble when the bubble was fully expanded. However, when the bubble was compressed, it hardly induced bending in the membrane as indicated by the stability of $D(t)$. This suggests that the water flow is not strong enough to pull the membrane toward the bubble. We calculated the nematic order parameter⁴⁵ of the unit vectors connecting GL1-C4A and GL2-C4B beads (see Figure 1A for schematic), and as seen in Figure 2B,

P_2 is stable, suggesting that the structure of the membrane is ordered and hardly affected by the bubble cavitation.

Now, we estimate the wall shear stress on the membrane caused by water flow. In order to estimate this value, we calculated, along the z -axis, from configurations in which the bubble was fully expanded, the average water velocity $v_{xy}(z)$ component in the direction parallel to the membrane. The average velocity is shown in Figure 2C, together with the distribution of the positions of the lipids. As seen, water near the membrane ($z \sim 18$ and 42 nm) slows down compared to the velocity of water near the bubble surface. The gradient in the water velocity produces a shear stress on the membrane, which is calculated as⁴⁶ $S = \eta(dv_{xy}(z)/dz)$, where η is the water viscosity, and for the MARTINI water, $\eta = 7 \times 10^{-4}$ Pa s.^{36,37} A linear data fit of $v_{xy}(z)$ (Figure 2C) yields a slope of $dv_{xy}(z)/dz = 0.5 \times 10^{-5}$ ps⁻¹, thus the wall shear stress is $S = 3500$ Pa.

As a qualitative comparison, we calculated the wall shear stress employing the theory developed by Nyborg.⁴⁷ According to this theory, the maximal shear stress exerted on a rigid plane by acoustic microstreaming produced by a hemispherical vibrating bubble attached to the plane is represented as

$$S^* = 2\pi^{3/2}(R - R_0)^2(\rho\omega^3\eta)^{1/2}/R_0 \quad (5)$$

where $(R - R_0)$ is the amplitude of the instantaneous radius of a vibrating bubble. The method was used to calculate the shear stress near a cell membrane by considering a cell as a solid boundary.^{10,17,48} With the values used in the simulation, $\rho = 10^3$ kg m⁻³, $\omega = 230$ MHz, $\eta = 7 \times 10^{-4}$ Pa s, and $R_0 = 8$ nm, we plot in Figure 3A the theoretical shear stress S^* as a function of the bubble's vibrating amplitude.

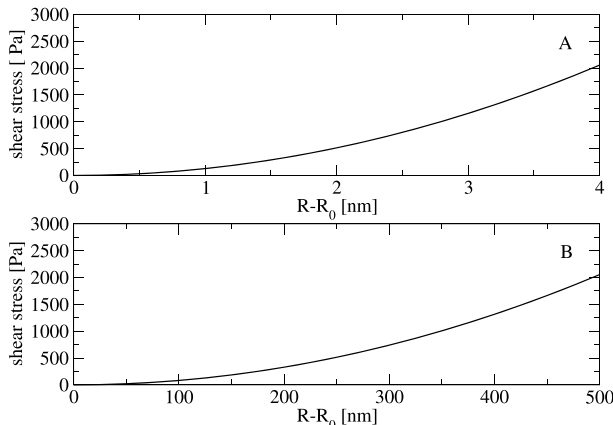


Figure 3. Theoretical wall shear stress as a function of the bubble's vibrational amplitude calculated using eq 5. Shown are the results for bubbles with equilibrium radii of $R_0 = 8$ nm and vibrating with frequencies of $\omega = 230$ MHz ($\tau = 4.3$ ns) (A), and $R_0 = 1 \mu\text{m}$ and vibrating with a frequency of $\omega = 5$ MHz ($\tau = 0.2 \mu\text{s}$) (B).

As seen in Figure 3, when the bubble reaches its maximum size of $R_{\max} = 12$ nm, corresponding to the $R - R_0$ amplitude of 4 nm, the shear stress is $S^* \sim 2000$ Pa. Given the rigid membrane assumption and the linear approximation in the theory, the agreement between the NEMD simulation and theoretical shear stresses is quite reasonable. This allows us to compare our results with that obtained using microscale parameters used in experiments. Typical experimental values of the equilibrium bubble radii and ultrasound frequencies are $R_0 = 0.5\text{--}5 \mu\text{m}$ and $\omega = 0.5\text{--}10$ MHz, respectively. Let us

consider an example case with $R_0 = 1 \mu\text{m}$, $\omega = 5$ MHz, and the bubble oscillates between $R_{\max} = 1.5 \mu\text{m}$ and $R_{\min} = 0.5 \mu\text{m}$. We assume that living cells are surrounded by whole blood, thus we take the value of the blood viscosity $\eta_{\text{blood}} = 3 \times 10^{-3}$ Pa.⁴⁸ The shear stress induced by this bubble cavitation as a function of the vibrating amplitude is shown in Figure 3B. This is an important result that allows us to bridge the gap between our simulations and experiments. A nanosized bubble vibrating with a nanosecond period (Figure 3A) produces similar wall shear stress as a microsized bubble vibrating with a slower microsecond period (Figure 3B). We should note that our estimated shear stress values are of the same order of magnitude as those reported based on complicated continuum mathematical models.^{17,49-52} Our simulations show that the membrane is hardly affected by the wall shear stress of ~ 3500 Pa, suggesting that water flow, generated by the bubble cavitation, may not be what induces the formation of a membrane pore, at least not at the very beginning of the ultrasound exposure. Since this shear stress is substantially above the physiological regime of $2\text{--}10$ Pa,⁵³ the experimentally observed crossing of drugs from bubbles into cells may be caused by biological processes rather than mechanical processes. For instance, shear stress may stimulate endocytosis, and this may be how a cell uptakes drugs bound to its surface.

Effect of the Bubble–Membrane Interaction on the Membrane Pore Formation. Now, we wish to investigate the role of the attractive interaction between the bubble and membrane on the formation of a pore. In order to investigate this, we carried out a 280 ns NEMD simulation, where eq 2 includes both interactions between the bubble with the membrane and water. All parameters are kept the same as those used in the simulation presented previously. Figure 4A shows the time evolution of the bubble radius $R(t)$ and the shortest distance $D(t)$ between the bubble center and the membrane. Their behavior is rather complicated. Initially, $R_0 = 8$ nm, $D = 12$ nm, i.e., the membrane was ~ 4 nm away from the bubble surface, and there was no direct interaction between them, as shown by the zero potential energy in Figure 4B. Following the bubble contraction, water flowed toward the bubble's center, inducing a slight bending of the membrane toward the bubble. When the bubble was fully compressed to $R_{\min} = 4$ nm at $t = 1.07$ ns, the membrane was still ~ 8 nm away from the bubble surface, thus the potential energy remained zero. Then, the expansion of the bubble exerted pressure on the water, which in turn pushed the membrane further away. At $t = 3.22$ ns, the bubble was fully expanded with $R_{\max} = 12$ nm and close enough to interact directly with the membrane, as reflected by the decrease in the potential energy (eq 2) from 0 to $\sim -1.25 \times 10^5$ kJ/mol (Figure 4B). Because of this direct attractive interaction, during the next contraction, the bubble strongly pulls the membrane toward it. At $t \sim 4.22$ ns, the bubble is at equilibrium, and the membrane is significantly bent with $D \sim 7$ nm, as seen from a snapshot in Figure 4C. However, at this state, the membrane elastic potential resists against the pulling of the bubble. Consequently, in the next vibrational period, while the bubble continues to be compressed to the minimum size, $R_{\min} = 4$ nm at $t = 5.29$ ns, the membrane does not follow the bubble, but restores to the initial position with $D \sim 12$ nm. Then, the bubble expands and gets closer to the membrane, thus the attractive potential becomes stronger (Figure 4B), pulling and inducing the bending of the membrane. At $t = 6.45$ ns, the bubble is at equilibrium, and $D(t) \approx R_0 = 8$ nm. This indicates that some

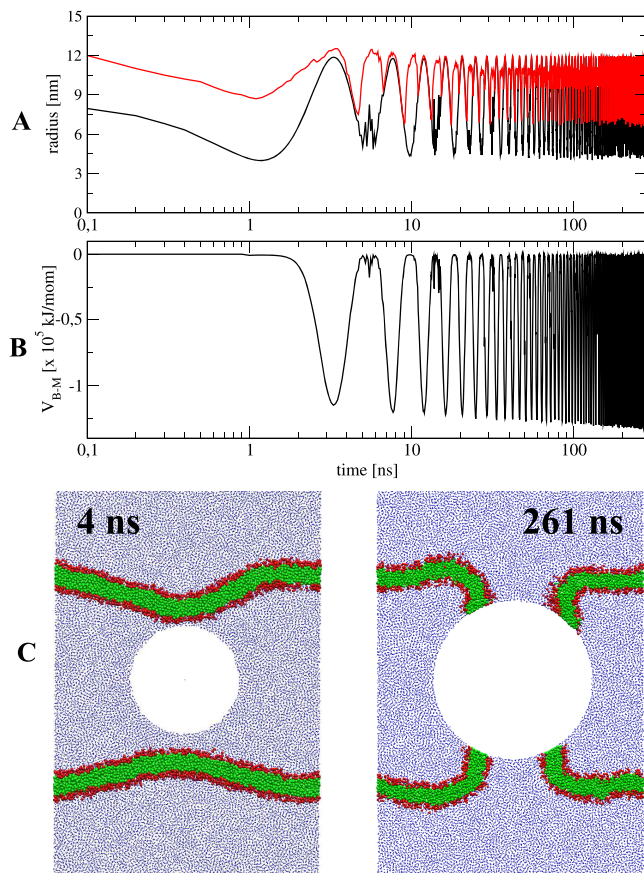


Figure 4. Time evolution of the bubble's radius (black) and the shortest distance between the bubble's center to the membrane (red) (A), and the interaction potential energy between the bubble and the membrane (B). The cross section of two selected snapshots before and after pore formation (C). For clarity, the *x*-axis in (A) and (B) is shown by log-scale.

lipids are attached to the bubble surface. Then, the bubble continued to expand, pushing the membrane back to the initial position. As this process was repeated over many vibrational periods, more and more lipids were pulled out of the membrane and attached to the bubble surface. This is seen from a decrease in the bubble-membrane potential energy from -1.25×10^5 to -1.30×10^5 kJ/mol after 30 ns (Figure 4B). Finally, after a large amount of lipid molecules had been pulled out of the membrane, a pore was formed, as seen in a representative snapshot shown in Figure 4C at $t = 261$ ns. Figure 5 shows the distribution of the positions of the atoms in the OXZ plan. As seen, a pore starts to open after around 30

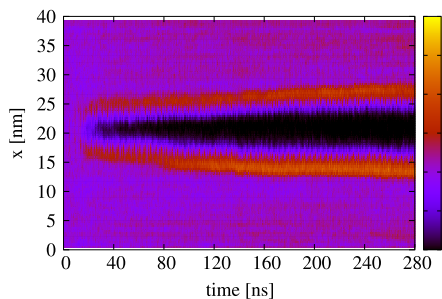


Figure 5. Time evolution of the distribution of positions of the lipid beads in the OXZ plan.

ns, quickly increasing in size, and reaches a diameter of ~ 8 nm after 280 ns.

As seen in Figure 4C at 261 ns, despite the opening of a pore in the membrane, the bubble may prevent the transport of molecules across the pore, i.e., the bubble plays the role of a lid. However, this is due to the bubble center being fixed during the simulation. In reality, bubbles always move, thus the pore is unblocked after the bubble moves to another place or collapses. To verify, we took the final system configuration at 280 ns, removed the bubble, and carried out an equilibrium MD simulation in the *NPT* ensemble at the ambient conditions of $T = 300$ K and $P = 1$ bar for 840 ns. The Berendsen semi-isotropic pressure coupling method was employed with the pressure coupling constant of 10 ps.

Figure 6A shows the time-evolution of the water density inside the spherical cavity with the radius of 8 nm previously

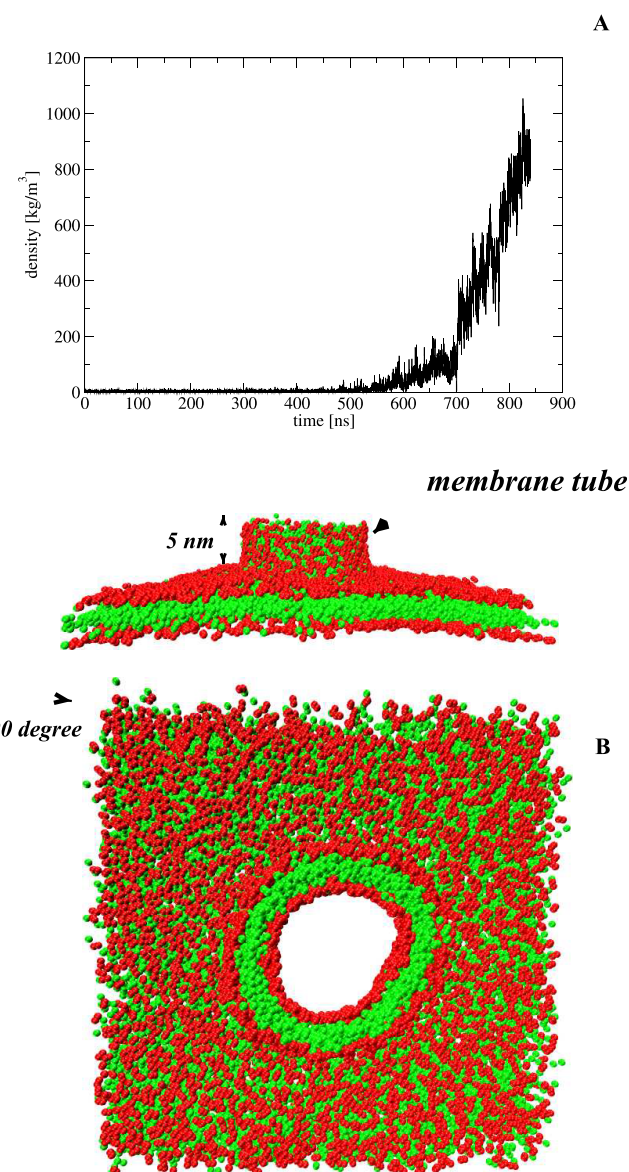


Figure 6. Time evolution of the water density inside the spherical cavity with an initial radius of 8 nm (A), and a snapshot of the membrane at 840 ns. Shown are the results obtained from the equilibrium simulation without the bubble. The membrane tube with length of ~ 5 nm is indicated.

occupied by the bubble. As seen, the cavity is stable up to ~500 ns and then quickly collapses, as indicated by the increase of the water density to ~850 kg/m³ at 840 ns. Interestingly, the pore in the membrane remained open during this time. We analyzed the pore structure in detail, and the final snapshot seen in Figure 6B shows that lipids, which were pulled out of the membrane during bubble contraction, tend to form a stable membrane tube perpendicular to the membrane. This tube was found to be ~5 nm and remained attached to the membrane. This prevents the assembly of lipids in the membrane to close the pore. Consequently, the closing of the pore is expected to take a very long time.

Finally, we should mention, that there is another mechanism which suggests that gas bubbles are formed within the membrane due to the nucleation² or the separation of bilayer leaflets under ultrasound.⁵⁴ These bubbles subsequently grow, expand, and collapse, creating pores in the membrane. Our mechanism is different, it does not require the intramembrane bubble nucleation. The fusion of the lipid-coated bubble with the membrane results in the membrane–bubble complex, and the stable cavitation of the bubble is sufficient to create a pore in the membrane.

CONCLUDING REMARKS

We have carried out NEMD simulations to investigate the role of water flow on the wall shear stress and the direct attractive interaction between the bubble and the membrane on the formation of pores in a model DOPC lipid bilayer. We show that both our computational nanobubble, vibrating with a nanosecond time scale, and experimental microbubbles, vibrating with microsecond period time scales, produce similar wall shear stress on the membrane. Since this shear stress, which is in the order of thousands of Pa, does not induce the formation of a pore in the membrane, we suggest that it probably does not play a direct role in the delivery of drugs across the cell membrane observed in experiments, at least not in the very early stages. In contrast, the direct interaction between the bubble's surface with the membrane pulls lipid molecules out of the membrane surface upon the compression of the bubble, creating a membrane pore after many cavitation periods. We believe that this is a generic mechanism which plays a dominant role in the bubble cavitation-induced membrane pore formation. However, the time scale of the opening process should depend on (i) the bubble surface material, which specifies both the resonance frequency of the bubbles and the interaction strength with the cell membrane, and (ii) the distance between the bubbles and the membrane. The bubble–membrane attractive interaction in this study is represented by a mean field potential, whose strength is described by a single average value. With these bubble and DOPC membrane models, the pore is formed quickly within nanosecond time scales when the bubble is placed close to the membrane. In reality, bubbles are made from different materials and vibrate with microsecond periods, thus the opening times could be different. Our simulations suggest that while a pore in the membrane can be formed by pulling of lipids out of the membrane by a contracting bubble, these lipids will form a stable membrane tube that remains attached to the membrane. This suggests that pore closing may be a slow process. The pores may remain open long enough for drugs to cross the cell membrane; however, unwanted toxic molecules may also enter the cells, causing side effects. When bubbles are largely compressed or even collapse, then lipids

completely detach from the membrane. In this case, a membrane tube would not be formed, and the lipids inside the membrane may quickly rearrange to close the pore. This suggests experimentalist could optimize various parameters, such as bubble shell material, size of the bubble shell, ultrasound frequency, and intensity, such that the opening and closing of the pore can be controlled. We are currently running simulations with different frequencies, interaction strengths, and bubble sizes to find the best combination of parameters.

AUTHOR INFORMATION

Corresponding Authors

*E-mail: philippe.derreumaux@tdtu.edu.vn.

*E-mail: nguyen@ibpc.fr.

ORCID

Viet Hoang Man: 0000-0002-8907-6479

Mai Suan Li: 0000-0001-7021-7916

Philippe Derreumaux: 0000-0001-9110-5585

Phuong H. Nguyen: 0000-0003-1284-967X

Notes

The authors declare no competing financial interest.

ACKNOWLEDGMENTS

The authors would like to thank Dr. Dominik Domin for reading the manuscript and his revision suggestions. This work has been supported by the CNRS, the Department of Science and Technology at Ho Chi Minh City, Vietnam (Grant 33/2017/HD-KHCNTT), Polish NCN Grant 2015/19/B/ST4/02721, and the National Institutes of Health (R01-GM079383, R21-GM097617, and P30-DA035778). The content is solely the responsibility of the authors and does not necessarily represent the official views of the National Institutes of Health or other funding organizations. Computational support from the IDRIS, CINES, and TGCC centers (Project A0040710411); the Center for Research Computing of University of Pittsburgh; and the Extreme Science and Engineering Discovery Environment (CHE090098, MCB170099 and MCB180045P) is acknowledged.

REFERENCES

- (1) Rodriguez-Rodriguez, J.; Sevilla, A.; Martinez-Bazan, C.; Gordillo, J. M. Generation of Microbubbles with Applications to Industry and Medicine. *Annu. Rev. Fluid Mech.* **2015**, *47*, 405–429.
- (2) Schroeder, A.; Kost, J.; Barenholz, Y. Ultrasound, Liposomes, and Drug Delivery: Principles for Using Ultrasound to Control the Release of Drugs From Liposomes. *Chem. Phys. Lipids* **2009**, *162*, 1–16.
- (3) Wrenn, S. W.; Dicker, S. M.; Small, E. F.; Dan, N. R.; Mleczko, M.; Schmitz, G.; Lewin, P. A. Bursting Bubbles and Bilayers. *Theranostics* **2012**, *2*, 1140.
- (4) Hyynnen, K.; McDannold, N.; Vykhotseva, N.; Jolesz, F. A. Noninvasive MR Imaging-Guided Focal Opening of the Blood-Brain Barrier in Rabbits. *Radiology* **2001**, *220*, 640.
- (5) Meairs, S. Facilitation of Drug Transport across the Blood-Brain Barrier with Ultrasound and Microbubbles. *Pharmaceutics* **2015**, *7*, 275.
- (6) Aryal, M.; Arvanitis, C. D.; Alexander, P. M.; McDannold, N. Ultrasound-Mediated Blood–Brain-Barrier Disruption for Targeted Drug Delivery in the Central Nervous System. *Adv. Drug Delivery Rev.* **2014**, *72*, 94–109.
- (7) Brennen, C. E. *Cavitation and Bubble Dynamics*; University Press: Oxford, 1995.

- (8) Nyborg, W. Ultrasound, Contrast Agents and Biological Cells; A simplified Model for Their Interaction During in vitro Experiments. *Ultrasound Med. Biol.* **2006**, *32*, 1557–1568.
- (9) Doinikov, A.; Dayton, P. Maxwell Rheological Model for Lipid-Shelled Ultrasound Microbubble Contrast Agents. *J. Acoust. Soc. Am.* **2007**, *121*, 3331–3340.
- (10) Doinikov, A.; Bouakaz, A. Theoretical Investigation of Shear Stress Generated By a Contrast Microbubble on the Cell Membrane as a Mechanism for Sonoporation. *J. Acoust. Soc. Am.* **2010**, *128*, 11–19.
- (11) Delalande, A.; Kotopoulos, S.; Rovers, T.; Pichon, C.; Postema, M. Sonoporation at a Low Mechanical Index. *Bubble Sci., Eng., Technol.* **2011**, *3*, 3–12.
- (12) Lee, S.; Anderson, T.; Zhang, H.; Flotte, T. J.; Doukas, A. G. Alteration of Cell Membrane by Stress Waves in vitro. *Ultrasound Med. Biol.* **1996**, *22*, 1285.
- (13) Lokhandwala, M.; Sturtevant, B. Mechanical Haemolysis in Shock Wave Lithotripsy (SWL): I. Analysis of Cell Deformation Due to SWL Flow-Fields. *Phys. Med. Biol.* **2001**, *46*, 413.
- (14) Zarnitsyn, V. G.; Prausnitz, M. R. Physical Parameters Influencing Optimization of Ultrasound-Mediated DNA Transfection. *Ultrasound Med. Biol.* **2004**, *30*, 527–538.
- (15) Lin, H. Y.; Thomas, H. L. Factors Affecting Responsivity of Unilamellar Liposomes to 20 kHz Ultrasound. *Langmuir* **2004**, *20*, 6100–6106.
- (16) Schlicher, R. K.; Radhakrishna, H.; Tolentino, T. P.; Apkarian, R. P.; Zarnitsyn, V.; Prausnitz, M. R. Mechanism of Intracellular Delivery by Acoustic Cavitation. *Ultrasound Med. Biol.* **2006**, *32*, 915–924.
- (17) Wu, J. Theoretical Study on Shear Stress Generated by Microstreaming Surrounding Contrast Agents Attached to Living Cells. *Ultrasound Med. Biol.* **2002**, *28*, 125–129.
- (18) Wu, J.; Ross, J.; Chiu, J. Reparable Sonoporation Generated by Microstreaming. *J. Acoust. Soc. Am.* **2002**, *111*, 1460–1464.
- (19) Marmottant, P.; Hilgenfeldt, S. Controlled Vesicle Deformation and Lysis by Single Oscillating Bubbles. *Nature* **2003**, *423*, 153–156.
- (20) Wu, J. Shear Stress in Cells Generated by Ultrasound. *Prog. Biophys. Mol. Biol.* **2007**, *93*, 363.
- (21) Wu, J.; Nyborg, W. L. Ultrasound, Cavitation Bubbles and Their Interaction With Cells. *Adv. Drug Delivery Rev.* **2008**, *60*, 1103.
- (22) Pong, M.; Umchid, S.; Guarino, A. J.; Lewin, P. A.; Litniewski, J.; Nowicki, A.; Wrenn, S. P. In vitro Ultrasound-Mediated Leakage From Phospholipid Vesicles. *Ultrasonics* **2006**, *45*, 133–145.
- (23) Shervani-Tabar, M.; Aghdam, A. H.; Khoo, B.; Farhangmehr, V.; Farzaneh, B. Numerical Analysis of a Cavitation Bubble in the Vicinity of an Elastic Membrane. *Fluid Dyn. Res.* **2013**, *45*, 055503.
- (24) Ganzenmüller, G. C.; Hiermaier, S.; Steinhäuser, M. O. ShockWave Induced Damage in Lipid Bilayers: A Dissipative Particle Dynamics Simulation Study. *Soft Matter* **2011**, *7*, 4307–4317.
- (25) Choubey, A.; Vedadi, M.; Nomura, K.; Kalia, R. K.; Nakano, A.; Vashishta, P. Poration of Lipid Bilayers by Shock-Induced Nanobubble Collapse. *Appl. Phys. Lett.* **2011**, *98*, 023701.
- (26) Schanz, D.; Metten, B.; Kurz, T.; Lauterborn, W. Molecular Dynamics Simulations of Cavitation Bubble Collapse and Sonoluminescence. *New J. Phys.* **2012**, *14*, 113019.
- (27) Nomura, K.; Kalia, R. K.; Nakano, A.; Vashishta, P.; Shekhar, A. Nanobubble Collapse on a Silica Surface in Water: Billion-Atom Reactive Molecular Dynamics Simulations. *Phys. Rev. Lett.* **2013**, *111*, 184503.
- (28) Koshiyama, K.; Kodama, T.; Yano, T.; Fujikawa, S. Structural Change in Lipid Bilayers and Water Penetration Induced by Shock Waves: Molecular Dynamics Simulations. *Biophys. J.* **2006**, *91*, 2198–2205.
- (29) Santo, K. P.; Berkowitz, M. L. Shock Wave Induced Collapse of Arrays of Nanobubbles Located Next to a Lipid Membrane: Coarse Grained Computer Simulations. *J. Phys. Chem. B* **2015**, *119*, 8879–8889.
- (30) Santo, K. P.; Berkowitz, M. L. Shock Wave Interaction with a Phospholipid Membrane: Coarse-Grained Computer Simulations. *J. Chem. Phys.* **2014**, *140*, 054906.
- (31) Fu, H.; Comer, J.; Cai, W.; Chipot, C. Sonoporation at Small and Large Length Scales: Effect of Cavitation Bubble Collapse on Membranes. *J. Phys. Chem. Lett.* **2015**, *6*, 413–418.
- (32) Koshiyama, K.; Wada, S. Collapse of a Lipid-Coated Nanobubble and Subsequent Liposome Formation. *Sci. Rep.* **2016**, *6*, 28164.
- (33) Viet, M. H.; Derreumaux, P.; Nguyen, P. H. Nonequilibrium All-Atom Molecular Dynamics Simulation of the Ultrasound Induced Bubble Cavitation and Application to Dissociate Amyloid Fibril. *J. Chem. Phys.* **2016**, *145*, 174113.
- (34) Viet, M. H.; Li, M.; Derreumaux, P.; Nguyen, P. H. Rayleigh-Plesset Equation of the Bubble Stable Cavitation in Water: A Nonequilibrium All-Atom Molecular Dynamics Simulation Study. *J. Chem. Phys.* **2018**, *148*, 094505.
- (35) Sirsi, S.; Borden, M. Microbubble Compositions, Properties and Biomedical Applications. *Bubble Sci., Eng., Technol.* **2009**, *1*, 3–17.
- (36) Marrink, S. J.; Risselada, J.; Yefimov, S.; Tieleman, D. P.; de Vries, A. H. The MARTINI Force Field: Coarse Grained Model for Biomolecular Simulations. *J. Phys. Chem. B* **2007**, *111*, 7812–7824.
- (37) Marrink, S. J.; Tieleman, D. P. Perspective on the MARTINI. *Chem. Soc. Rev.* **2013**, *42*, 6801–6822.
- (38) Marrink, S. J.; Mark, A. E. The Mechanisms of Vesicle Fusion As Revealed by Molecular Dynamics Simulations. *J. Am. Chem. Soc.* **2003**, *125*, 11144.
- (39) Lindahl, E.; Hess, B.; van der Spoel, D. GROMACS 3.0: A Package for Molecular Simulation and Trajectory Analysis. *J. Mol. Model.* **2001**, *7*, 306–317.
- (40) Sassaroli, E.; Hynynen, K. Resonance Frequency of Microbubbles in Small Blood Vessels: A Numerical Study. *Phys. Med. Biol.* **2005**, *50*, 5293–5305.
- (41) Adamson, A. W.; Gast, A. P. *Physical Chemistry of Surfaces*; Wiley: New York, 1997.
- (42) Berendsen, H. J. C.; Postma, J. P. M.; van Gunsteren, W. F.; Dinola, A.; Haak, J. R. Molecular-Dynamics With Coupling to an External Bath. *J. Chem. Phys.* **1984**, *81*, 3684–3690.
- (43) Darden, T.; York, D.; Pedersen, L. Particle Mesh Ewald: An N-log(N) Method for Ewald Sums in Large Systems. *J. Chem. Phys.* **1993**, *98*, 10089–10092.
- (44) Marrink, S. J.; Periole, X.; Tieleman, D. P.; de Vries, A. H. Comment on: On Using a Too Large Integration Time Step in Molecular Dynamics Simulations of Coarse-Grained Molecular Models. *Phys. Chem. Chem. Phys.* **2010**, *12*, 2254.
- (45) Nguyen, P.; Li, M. S.; Straub, J. E.; Thirumalai, D.; Stock, G. Monomer Adds to Preformed Structured Oligomers of $\text{A}\beta$ -Peptides by a Two-Stage Dock-Lock Mechanism. *Proc. Natl. Acad. Sci. U. S. A.* **2007**, *104*, 111–116.
- (46) Volino, R. J.; Schultz, M. P. Determination of Wall Shear Stress from Mean Velocity and Reynolds Shear Stress Profiles. *Phys. Rev. Fluids* **2018**, *3*, 034606.
- (47) Nyborg, W. L. Acoustic Streaming near a Boundary. *J. Acoust. Soc. Am.* **1958**, *30*, 329.
- (48) Lewin, P. A.; Bjorno, L. Acoustically Induced Shear Stresses in the Vicinity of Microbubbles in Tissue. *J. Acoust. Soc. Am.* **1982**, *71*, 728.
- (49) Hosseinkhah, N.; Hynynen, K. A Three-Dimensional Model of an Ultrasound Contrast Agent Gas Bubble and its Mechanical Effects on Microvessels. *Phys. Med. Biol.* **2012**, *57*, 785–800.
- (50) Wiedemair, W.; Tukovic, Z.; Jasak, H.; Poulikakos, D.; Kurtcuoglu, V. On Ultrasound-Induced Microbubble Ossillation in a Capillary Blood Vessel and its Implications for the Blood-Brain Barrier. *Phys. Med. Biol.* **2012**, *57*, 1019–1045.
- (51) Hosseinkhah, N.; Chen, H.; Matula, T.; Burns, P. N.; Hynynen, K. Mechanisms of Microbubble-Vessel Interactions and Induced Stresses: A Numerical Study. *J. Acoust. Soc. Am.* **2013**, *134*, 1875–1885.

(52) Hosseinkhah, N.; Goertz, D. E.; Hyynnen, K. Microbubbles and Blood-Brain Barrier Opening: A Numerical Study on Acoustic Emissions and Wall Stress Predictions. *IEEE Trans. Biomed. Eng.* **2015**, *62*, 1293–1304.

(53) Reneman, R. S.; Arts, T.; Hoeks, A. P. Wall Shear Stress—an Important Determinant of Endothelial Cell Function and Structure—in the Arterial System *in vivo*. Discrepancies with Theory. *J. Vasc. Res.* **2006**, *43*, 251.

(54) Krasovitski, B.; Frenkel, V.; Shoham, V.; Kimmel, E. Intramembrane Cavitation as a Unifying Mechanism for Ultrasound-Induced Bioeffects. *Proc. Natl. Acad. Sci. U. S. A.* **2011**, *108*, 3258.